MOX-Report No. 48/2016

Shear Stress Alterations in the Celiac Trunk of Patients with Continuous-Flow Left Ventricular Assist Device by In-Silico and In-Vitro Flow Analysis

Scardulla, S.; Pasta, S.; D'Acquisto, L.; Sciacca, S.; Agnese, V.; Vergara, C.; Quarteroni, A.; Clemenza, F.; Bellavia, D.; Pilato, M.

MOX, Dipartimento di Matematica
Politecnico di Milano, Via Bonardi 9 - 20133 Milano (Italy)

mox-dmat@polimi.it http://mox.polimi.it

Shear Stress Alterations in the Celiac Trunk of Patients with Continuous-Flow Left Ventricular Assist Device by In-Silico and In-Vitro Flow Analysis

Francesco Scardulla[1], Salvatore Pasta[2,3], Leonardo D'Acquisto[1], Sergio Sciacca[3], Valentina Agnese[3], Christian Vergara[4], Alfio Quarteroni[4,5], Francesco Clemenza[3], Diego Bellavia[3], and Michele Pilato[3]

[1] Dipartimento dell'Innovazione Industriale e Digitale (DIID), Università di Palermo, Palermo, Italy

[2] Fondazione Ri.MED, Palermo, Italy

[3] Department for the Treatment and Study of Cardiothoracic Diseases and Cardiothoracic Transplantation (IRCCS-ISMETT), Palermo, Italy

[4] MOX, Dipartimento di Matematica, Politecnico di Milano, Milan, Italy

[5] SB MATHICSE CMCS, École polytechnique fédérale de Lausanne, Lausane, Switzerland

Corresponding author:
Salvatore Pasta, PhD
National Scientific Qualification as Professor in Mechanical Engineering,
Fondazione Ri.MED
Phone: +39 091 3815681
FAX: +39 091 3815682
e-mail: spasta@fondazionerimed.com

Abstract

Background: The use of left ventricular assist device (LVAD) to treat advanced cardiac heart failure is constantly increasing, although this device leads to high risk for gastrointestinal.

Methods: Using *in-silico* flow analysis, we quantified hemodynamic alterations due to continuous-flow LVAD (HeartWare Inc, Framingham, MA, USA) in the celiac trunk and major branches of the abdominal aorta and then explored the relationship between wall shear stress (WSS) and celiac trunk orientation. To assess outflow from aortic branch, a 3D printed patient-specific model of the celiac trunk reconstructed from a LVAD-supported patient was used to estimate echocardiographic outflow velocities under continuous-flow conditions and then to calibrate computational simulations. Moreover, flow pattern and resulting WSS were computed on 5 patients with LVAD implantation.

Results: Peak WSSs were estimated on the three branches of celiac trunk and the LVAD cannula. Mean values of WSS demonstrated that the left gastric artery experiences the greatest WSS of 9.08±5.45 Pa with an average flow velocity of 0.57±0.25 m/s when compared to that of other vessel districts. The common hepatic artery had the less critical WSS of 4.58±1.77 Pa. A positive correlation was found between the celiac trunk angulation and the WSS stress just distal the ostium of celiac trunk (R=0.9), and this may increase to vulnerability of this vessel to bleeding.

Conclusions: Although further studies are warranted to confirm these findings in a larger patient cohort, computational flow simulations may enhance the information of clinical image data and may have an application in clinical investigations of hemodynamic changes in LVAD-supported patients.

Keywords— left ventricular assist device (LVAD); gastrointestinal bleeding; computational fluid dynamics; abdominal aorta; celiac trunk.

1. Introduction

Heart transplantation is the gold-standard therapy for patients with heart failure. Unfortunately heart donors are limited, and alternative methods are needed to treat advanced end-organ failure. The use of left ventricular assist devices (LVADs) is gaining more acceptance as a bridge to transplant, bridge to decision or final “destination therapy”, making patients survive on mechanical support (1, 2). Since these devices may profoundly impact the hemodynamics of entire aorta, especially if support is provided by a continuous flow pump system, there is an urgent need to better understand these alterations and the consequent response of the cardiovascular system. These responses may include short- and long-term postoperative complications after LVAD implantation including renal dysfunction (3), neurological complications (4) and infection (5). Among these, gastrointestinal bleeding presents with a range of 11-65% within the first year of LVAD placement (6-8), and treatment options include anticoagulant/antiplatelets drugs suspension, endoscopic treatment, bowel resection, cardiac transplantation (9). As in severe aortic stenosis, the continuous pump action of the mechanical support may determine a deficiency of the high-molecular weight multimer of von Willebrand factor (10, 11), which predisposes patients to bleeding *via* a hemodynamic-mediated mechanism (12, 13). Assessment of LVAD-induced wall shear stress (WSS) may partially provide explanations on the development of bleeding.

Although hemodynamic measurements can be obtained non-invasively by magnetic resonance imaging (MRI), LVAD devices are not MRI-compatible. An alternative and feasible option is the use of *in-silico* simulations, and here computational flow analysis offers the unique opportunity to simulate hemodynamics and derive quantitative parameters such as WSS in LVAD-supported patients. The shear stress represents the frictional force exerted by the flowing blood on the intimal surface of vessel wall and promotes arterial disease when its value falls above or below the normal, physiologic range (14). Computational flow analysis has previously been successful in revealing distinct features of altered hemodynamic in cardiovascular diseases such as aortic aneurysms (15-17) and dissections (18, 19).

Computational flow analysis was used in the current study to characterize potentially adverse hemodynamic conditions in the celiac trunk and major branches of the abdominal aorta in five patients

with continuous-flow LVAD devices as well as to explore the relationship of the shear stress magnitude with the anatomic orientation of the celiac trunk. We retain that altered WSS magnitude in the celiac trunk wall may trigger biochemical mechanisms causing the development of gastrointestinal bleeding since high WSS may damage the high-molecular weight multimers of von Willebrand factor. Outflow conditions from aortic branches were quantified by echocardiographic imaging on a 3D patient-specific celiac-trunk model under continuous-flow conditions by *in-vitro* testing and then used to calibrate computational simulations. This study is motivated by the occurrence of gastrointestinal bleeding in this patient study group.

2. Material and Methods

2.1 Patient Study Group

After IRB protocol approval and signed informed consent, 5 patients underwent contrast-enhanced computed-tomography angiography (CTA) following LVAD placement, and were enrolled to assess the putative cause of bleeding. CTA imaging was performed using a 64-slice scanner (VCT64; GE Healthcare, Milwaukee, WI, USA) with retrospective ECG gating (80% of R-R cycle). From the acquired volumetric data, the CTA scans were retro-reconstructed using a multisegment reconstruction algorithm and thin sections of 0.49-0.62 mm. The patient study group was composed of 4 male (cases A, B, C and E) and 1 female (case D), mean age 57±5 years. All patients were referred to LVAD implantation due to ischemic (n=3) and non-ischemic (n=2) dilatative cardiomyopathy. The time of LVAD implantation to CTA imaging was on average of 46 days (range, 21-75 days). The LVAD (HeartWare Inc, Framingham, Mass, USA) had a continuous flow in the range of 4-5 L/min. Patients B and E had gastrointestinal bleeding, patients B and C had right ventricular failure and patient E presented right common iliac artery thrombotic sub-occlusion. From CTA imaging, the azimuth angle of the celiac trunk centerline with that of descending aorta was measured for each patient, and then correlated to the shear stress.

2.2 Phantom and Flow circuit

To develop an experimentally-calibrated computational fluid-dynamic model (CFD), physiological flow splits in the celiac trunk branches were estimated using continuous-wave (CW) Doppler echocardiography on a patient-specific model of the aorta (case A). For the patient A, the aorta from

the ascending to distal celiac trunk, including the splenic, gastric and hepatic vessels, through the mesenteric artery ending at the left and right renal arteries was reconstructed from CTA scans using the vascular modeling toolkit ITK (v.0.9.0; http://www.vmtk.org). Then, the reconstructed patient-specific anatomy was manufactured by 3D printing technology (Materialise NV; Leuven, Belgium) to obtain a rigid, transparent flow channel of abdominal aorta (Figure 1). Surface polishing was performed to reduce inner layer roughness. Then, the 3D printed model (scale 1:1) was connected to a compliant and transparent silicone phantom model of the thoracic aorta described previously (20) (see Figure 1).

The continuous-flow circuit consisted of (i) the LVAD device, (ii) the phantom model of entire aorta with the celiac trunk and (iii) the fluid reserve, all connected by silicone tubes and plastic connectors (Figure 1). The inlet flow was imposed changing the pump rotation speed of LVAD device to investigate three different hemodynamic scenarios with cardiac output (CO) of 4, 5 and 6 L/min at mean aortic pressure of 80 mmHg. Specifically, peripheral resistances and aortic pressure were varied using adjustable valves placed distal to each outlet. Pressure was continuously measured by several pressure transducers (X5072 Druck, GE Measurement and Control), and thus recorded with LabVIEW software (National Instruments, Austin,TX, USA). For flow measurements, an electromagnetic flowmeter (Optiflux 5300C; Krohne, Duisburg, Germany) was placed on the plastic tube after the LVAD device. The circuit contained water at room temperature. We performed echocardiographic imaging with a high-end ultrasound scanner equipped with a X5-1 probe transducer (EPIQ 7, Philips Healthcare, Andover, Massachusetts). Grayscale was used to visualize structures of aortic branches, while velocities at each outlet of the abdominal aorta were acquired using CW Doppler for different inflow scenarios. In all cases, measurement acquisitions were carried out few minutes after perfusion to warrant a fully developed, non-turbulent flow regime. Starting from these velocity measures, flow divisions were then estimated from the cross-sectional area of each branch of the abdominal aorta.

2.3 Computational Fluid Dynamics Simulations

Computational flow analyses were carried out using an approach previously developed by our group to study hemodynamics in pathologies of the thoracic aorta (15, 18, 21). For each patient, both aortic

geometry and LVAD inflow cannula were segmented from post-operative CTA images using a semi-automatic threshold-based technique. Image noise and artefacts were reduced by applying a fast Fourier transform spatial band pass filter and realigning images with respect to the aortic centreline, respectively. Axial and coronal images were used to reconstruct the complex anatomy of the splenic, gastric and hepatic vessels as well as the mesenteric and renal arteries. A computational mesh was then created by discretization of the aortic fluid domain into a set of small elements with unstructured tetrahedral morphology (element size of 0.8 mm) using GAMBIT 2.3.6 (ANSYS Inc., Canonsburg, PA). Blood was treated as a Newtonian and incompressible fluid with a density of 1060 kg/m^3 and dynamic viscosity of $3.71x10^{-3}$ Pa x s. The aortic wall was assumed rigid with no slip whereas flow was assumed laminar as qualitatively appeared from the experimental echocardiographic imaging investigation. The Navier-Stokes equations governing fluid motion were solved using the computational fluid dynamics software FLUENT v14.0.0 (ANSYS Inc., Canonsburg, PA) assuming steady analysis. This is reasonable because the continuous-flow generated by the LVAD does not determine appreciable flow differences between systole and diastole (22). To obtain realistic results from simulations, inflow and outflow boundary conditions were imposed according to the LVAD experimental setting described in the previous section and to the corresponding echocardiographic measurements of aortic branches. For the patient A, inflow from the cannula was kept constant for the entire cardiac cycle according to the device settings chosen for each patient. Moreover, a steady nonsignificant aortic flow was assumed to be present at aortic valve inlet (2% of CO) as reported by others (22). For patient A, flow split division computed from the echocardiographic flow measurements were imposed in each branch of the aorta. In addition, for case A only, the effect of LVAD outflow on WSS distribution was investigated with three different levels of CO (i.e., 4, 5 and 6 L/min). For other patients, the inflow was set according to LVAD setting while flow divisions were imposed according to data from the perfusion testing performed for patient A. Post-processing of hemodynamic simulations was performed with Paraview (Kitware Inc., Clifton Park, NY).

3. Results

For the celiac trunk model of patient A, flow velocities were experimentally derived from ultrasound measurements at different LVAD inflow pump rotation speeds and then used to calculate flow splits in the celiac trunk branch (Table 1). The higher the inflow from the LVAD device, the greater the flow

velocity in each branch as assessed by echocardiography. Spectral evaluation of the CW Doppler profiles confirmed a fully-developed, continuous flow in all investigated vessels of the celiac trunk model (Figure 2).

Hemodynamic disturbances induced by the LVAD placement were investigated for CO=5 L/min by flow streamlines analysis and WSSs. Laminar flow with peak velocities in correspondence of the cannula and LVAD graft anastomosis site was observed for the case A for which boundary conditions were calibrated by perfusion experiments (Figure 3). Flow entering the ascending aorta and aortic arch was slightly disorganized, but returned laminar in the descending aorta and distal aortic branches. Pronounced flow velocities were also observed in the arterial tree of the celiac trunk but not in the renal arteries. Distribution of WSS evinced focally high values of shear stress in the LVAD graft anastomosis site and just after the ostium of the celiac trunk (Figure 3). It can be also observed that shear stress is influenced by the LVAD pump rotation speed (Figure 4). In particular, WSS values were more pronounced in three investigated points as the CO was increased. (P1, P2, P3 = 1.7, 2.6, 3.9 Pa at 4 L/min; P1, P2, P3 = 2.6, 3.4, 5.5 Pa at 5 L/min and P1, P2, P3 = 4.7, 8.3, 13.7 Pa at 6 L/min). As the CO dictated by the LVAD device increased, the regions of the vessel wall at greater shear stress were consistently large.

Similar flow pattern and WSS distribution were observed in the celiac trunk of other patients with continuous-flow LVAD (Figure 5). Patients B and E exhibited the highest velocity of the flow circulating in the gastric, hepatic and splenic arteries as well as the mesenteric artery. Patient A exhibited low laminar flow conditions in the arterial tree of the abdominal aorta. This flow changes are likely caused by the particular anatomy of the celiac trunk of each patient. Likewise, the distribution of WSS was marked in patient B and E as compared to that shown by other cases. Mean values of WSS demonstrated that the left gastric artery experiences the greatest WSS of 9.08±5.45 Pa with an average flow velocity of 0.57±0.25 m/s when compared to shear stress in the other vessel districts (see Table 2). Among celiac trunk branches, the common hepatic artery had the less critical shear stress with a mean value of 4.58±1.77 Pa. High mean values of WSS were observed in the mesenteric artery (8.16±3.88 Pa) whereas the distal abdominal aorta experiences low shear stress (2.14±1.89 Pa) and flow velocities (0.26±0.12 m/s).

A strong positive correlation of WSS with the morphological anatomy of the celiac trunk (as quantified by the azimuth angle of the celiac trunk with respect to the abdominal aortic centerline) was found (Figure 6). Indeed, patients A, C and D with celiac trunk orientation of ~120 degree had lower WSS magnitudes than those of patients B and E with angles of 145 and 173 degree, respectively.

4. Discussion

To our knowledge, this is the first study integrating ultrasound flow velocity measurements performed on a 3D printed anatomic model with computational flow analysis in order to derive personalized insights into the shear stress induced by the LVAD on the different branches of the celiac trunk. We demonstrated that shear stress in LVAD-supported patients differs among the branches of the celiac trunk, and stress magnitudes are likely associated to the anatomical orientation of this major branch of the abdominal aorta. This can have direct and possibly catastrophic clinical consequences because an altered shear stress environment may induce pathological degradation of the von Willebrand factor, thereby promoting LVAD-related complications as gastrointestinal bleeding (9).

All investigations of blood flow in different types of LVADs have been mainly focused on the shear stress, turbulence, and flow velocity of the LVAD cannula by numerical simulations (22-27). Karmonik et al. (22) compared flow patterns of lateral versus anterior insertion of LVAD outflow cannula and concluded that the anterior geometry of the anastomosis leads to less disorganized flow at the root of the supra-aortic vessels and no impingement pressure zones at the contralateral aortic wall. Later, they observed significant retrograde flow in the ascending aorta of LVAD-supported patients who developed aortic insufficiency as a major complication of the continuous-flow assist device (26). A relationship between the cannula orientation (azimuth and polar angle) and the resulting hemodynamic alterations (pressure gradients, WSS, and turbulent energy dissipation) with the occurrence of the aortic insufficiency was found. In the present analysis, we corroborated the altered shear stress distribution in the outflow cannula and, most importantly, observe that shear stress remains pronounced in the distal districts of the aorta including the splenic and gastric arteries of the celiac trunk. Moreover, we found a robust correlation between the celiac trunk orientation and the resulting WSS magnitude. Patients B with a pronounced angulation of the celiac trunk exhibited the

highest WSS because the flow jet of blood was accelerated in the lumen of the celiac trunk and thus collided the vessel wall distally. This likely caused the gastrointestinal bleeding seen clinical for patient B. While, patients A, C and D presented lower magnitudes of the flow jet and resulting WSS at the ostium of the celiac trunk when compared to that of patient B and E. Various authors (28, 29) have demonstrated histologic changes in the aortic wall in response to high shear stress caused by the relatively small conduit cross-section of LVAD cannula. In the ascending aortic wall of failing heart, histological analysis showed more elastic fiber fragmentation, smooth-muscle-cell disorientation and depletion, fibrosis, medial degenerative changes and atherosclerotic changes after continuous-flow LVAD support (transplantation or autopsy) than at the time of LVAD implantation (28). We here speculate a similar flow-mediated mechanism for the celiac trunk in which the LVAD-induced non-physiological blood flow in this relatively-small vessel may locally increase the shear stress causing a structural damage of the vessel wall integrity.

It is known that pulsatile flow exhibits more favorable hemodynamic conditions including reduced WSS and lower pressures when compared to that of continuous-flow LVAD. Cyclic stretch of smooth muscle cell *in-vitro* is directly responsible for the proliferation of endothelial cell, expression of contractile phenotype, and the production of autocrine growth factors (30). Notwithstanding, clinical applications of continuous-flow LVAD is increasing since this device is usually smaller and produce less frequent bleeding and infections (31), although the absence of pulse pressure may in turn increase systemic vascular resistances and afterload. The mechanism underlying gastrointestinal bleeding on long-term continuous flow mechanical support is multifactorial and includes variables as the effect blood interaction with the device surface, anticoagulation therapies and an altered shear stress which participates in the damage of von Willebrand factor. Therefore, it is important to understand the point at which shear stress becomes damaging and why the occurrence of bleeding differ among patients and types of LVADs (pulsatile vs continuous-flow). However, WSS is difficult to quantify since LVAD is not compatible with 4D MRI flow imaging or with *in-vitro* models. Using computational flow simulations, values of time average WSS over one cardiac cycle were barely ~2.0 Pa near the celiac trunk of the healthy human abdominal aorta (32) and ~1.0 Pa near the celiac trunk of abdominal aortic aneurysms with diameter < 5.0 cm (33). Magnitudes of WSS as derived by 4D flow MRI were found lower in patients with pancreaticoduodenal artery aneurysms concomitant with

celiac trunk stenosis when compared to those of healthy controls (WSS ~ 2.0 Pa) (34). Our findings indicate that WSSs in LVAD-supported patients are markedly higher than those suggested by these studies (see Table 2), and this may result in pathologic von Willebrand degradation by a shear-mediated mechanism well described in literature (10). Although this study is not exhaustive, we highlighted that computational flow simulations enhance the information of clinical image data and may have an application in clinical investigations of hemodynamic alterations induced by LVAD implantation.

Study Limitation

One of the major limitations of this study is the low number of patients investigated. LVAD-supported patients who require CT with contrast agent are rare since this imaging technique is commonly indicated in complicated procedures (35). For comparison purposes, it would be ideal to have CT scans pre- and post LVAD implantation to assess whether hemodynamic alterations are induced by the mechanical support or the patient aortic anatomies. Moreover, our patient study group included different LVAD-related complications. Once again, this patient population is rare, and it could be unethical to perform a prospective CT contrast-enhanced study with potential harmful effects for the patients. Outflow boundary conditions as determined for patient A were not specific for other cases, and this may impact WSS as this parameter is sensitive to flow conditions. Convergence analysis of mesh quality was not performed at this stage. However, this experimentally-calibrated computational flow model offers unique opportunity to simulate flow patterns in patients with LVAD implantation.

5. Conclusion

This study demonstrates that altered shear stress occurs in the arterial tree of the celiac trunk in patients with continuous-flow LVAD and that such hemodynamic parameter is affected by the orientation of this major branch of the abdominal aorta as well as the speed of the pump device. As mechanical support moves toward a final “destination therapy” in heart failure, more studies are needed to understand the pathophysiological mechanisms underlying the LVAD-related complications so that *in-silico* modeling may enhance the information available from medical imaging towards the use of personalized therapeutic strategies.

Acknowledgment

Francesco Scardulla thanks the Italian Ministry of Education, University and Research for supporting his research. Salvatore Pasta is grateful to the Fondazione RiMED for supporting his research on cardiovascular biomechanics. Alfio Quarteroni and Christian Vergara thank Piergiorgio Tozzi (CHUV, Lausanne, Swtizerland) for many inspiring discussions and his advises on this topic.

Figure Legends

Figure 1: Schematic of continuous-flow circuit showing snapshots of the aortic model and the 3D printed patient-specific celiac trunk model

Figure 2: Examples of echocardiographic measurements performed on (A) abdominal aorta just distal renal arteries and (B) mesenteric artery at LVAD flow rate of 5 L/min

Figure 3: Flow pattern and WSS distribution for the entire aorta of the patient A with CO=5 L/min; the inset in the middles shows flow streamlines for the major branches of the abdominal aorta

Figure 4: Maps of WSS in the celiac trunk at different LVAD pump rotation speeds and selected point magnitudes of WSS

Figure 5: Flow patterns (top row) and corresponding WSS distribution (bottom row) in the celiac trunk of each investigated patients

Figure 6: Correlation plot illustrating linear relationship between the celiac trunk orientation and the shear stress parameter

Reference

1. Mancini D, Colombo PC: Left Ventricular Assist Devices A Rapidly Evolving Alternative to Transplant. Journal of the American College of Cardiology 2015;65:2542-55.
2. Miller LW, Pagani FD, Russell SD, et al.: Use of a continuous-flow device in patients awaiting heart transplantation. New Engl J Med 2007;357:885-96.
3. Kamdar F, Boyle A, Liao K, Colvin-Adams M, Joyce L, John R: Effects of Centrifugal, Axial, and Pulsatile Left Ventricular Assist Device Support on End-Organ Function in Heart Failure Patients. J Heart Lung Transpl 2009;28:352-9.
4. Hagan K: LVADs help mend a broken heart. The Nurse practitioner 2010;35:28-36;.
5. Holman WL, Rayburn BK, McGiffin DC, et al.: Infection in ventricular assist devices: prevention and treatment. Ann Thorac Surg 2003;75:S48-57.
6. Slaughter MS, Rogers JG, Milano CA, et al.: Advanced heart failure treated with continuous-flow left ventricular assist device. N Engl J Med 2009;361:2241-51.
7. Aggarwal A, Pant R, Kumar S, et al.: Incidence and management of gastrointestinal bleeding with continuous flow assist devices. Ann Thorac Surg 2012;93:1534-40.
8. Eckman PM, John R: Bleeding and thrombosis in patients with continuous-flow ventricular assist devices. Circulation 2012;125:3038-47.
9. Islam S, Cevik C, Madonna R, et al.: Left ventricular assist devices and gastrointestinal bleeding: a narrative review of case reports and case series. Clin Cardiol 2013;36:190-200.
10. Bartoli CR, Dassanayaka S, Brittian KR, et al.: Insights into the mechanism(s) of von Willebrand factor degradation during mechanical circulatory support. J Thorac Cardiov Sur 2014;147:1634-43.
11. Crow S, John R, Boyle A, et al.: Gastrointestinal bleeding rates in recipients of nonpulsatile and pulsatile left ventricular assist devices. J Thorac Cardiovasc Surg 2009;137:208-15.
12. Vincentelli A, Susen S, Le Tourneau T, et al.: Acquired von Willebrand syndrome in aortic stenosis. N Engl J Med 2003;349:343-9.
13. Siedlecki CA, Lestini BJ, Kottke-Marchant KK, Eppell SJ, Wilson DL, Marchant RE: Shear-dependent changes in the three-dimensional structure of human von Willebrand factor. Blood 1996;88:2939-50.

14. Shaaban AM, Duerinckx AJ: Wall shear stress and early atherosclerosis: A review. American Journal of Roentgenology 2000;174:1657-65.
15. Rinaudo A, Pasta S: Regional variation of wall shear stress in ascending thoracic aortic aneurysms. P I Mech Eng H 2014;228:627-38.
16. Faggiano E, Antiga L, Puppini G, Quarteroni A, Luciani GB, Vergara C: Helical flows and asymmetry of blood jet in dilated ascending aorta with normally functioning bicuspid valve. Biomech Model Mechanobiol 2013;12:801-13.
17. Soudah E, Ng EYK, Loong TH, Bordone M, Pua U, Narayanan S: CFD Modelling of Abdominal Aortic Aneurysm on Hemodynamic Loads Using a Realistic Geometry with CT. Comput Math Method M 2013.
18. D'Ancona G, Lee JJ, Pasta S, et al.: Computational analysis to predict false-lumen perfusion and outcome of type B aortic dissection. J Thorac Cardiov Sur 2014;148:1756-8.
19. Yu SCH, Liu W, Wong RHL, Underwood M, Wang DF: The Potential of Computational Fluid Dynamics Simulation on Serial Monitoring of Hemodynamic Change in Type B Aortic Dissection. Cardiovasc Inter Rad 2016;39:1090-8.
20. Pasta S, Scardulla F, Rinaudo A, et al.: An In Vitro Phantom Study on the Role of the Bird-Beak Configuration in Endograft Infolding in the Aortic Arch. Journal of endovascular therapy : an official journal of the International Society of Endovascular Specialists 2016;23:172-81.
21. D'Ancona G, Amaducci A, Rinaudo A, et al.: Haemodynamic predictors of a penetrating atherosclerotic ulcer rupture using fluid-structure interaction analysis. Interact Cardiov Th 2013;17:576-8.
22. Karmonik C, Partovi S, Loebe M, et al.: Influence of LVAD Cannula Outflow Tract Location on Hemodynamics in the Ascending Aorta: A Patient-Specific Computational Fluid Dynamics Approach. Asaio Journal 2012;58:562-7.
23. Neidlin M, Corsini C, Sonntag SJ, et al.: Hemodynamic analysis of outflow grafting positions of a ventricular assist device using closed-loop multiscale CFD simulations: Preliminary results. J Biomech 2016;49(13):2718-25.
24. Bonnemain J, Malossi AC, Lesinigo M, Deparis S, Quarteroni A, von Segesser LK: Numerical simulation of left ventricular assist device implantations: comparing the ascending and the descending aorta cannulations. Medical engineering & physics 2013;35:1465-75.

25. Karmonik C, Partovi S, Schmack B, et al.: Comparison of Hemodynamics in the Ascending Aorta Between Pulsatile and Continuous Flow Left Ventricular Assist Devices Using Computational Fluid Dynamics Based on Computed Tomography Images. Artificial organs 2014;38:142-8.
26. Karmonik C, Partovi S, Loebe M, et al.: Computational fluid dynamics in patients with continuous-flow left ventricular assist device support show hemodynamic alterations in the ascending aorta. J Thorac Cardiov Sur 2014;147:1326-U323.
27. Caruso MV, Gramigna V, Rossi M, Serraino GF, Renzulli A, Fragomeni G: A computational fluid dynamics comparison between different outflow graft anastomosis locations of Left Ventricular Assist Device (LVAD) in a patient-specific aortic model. Int J Numer Meth Bio 2015;31.
28. Segura AM, Gregoric I, Radovancevic R, Demirozu ZT, Buja LM, Frazier OH: Morphologic changes in the aortic wall media after support with a continuous-flow left ventricular assist device. The Journal of heart and lung transplantation : the official publication of the International Society for Heart Transplantation 2013;32:1096-100.
29. Nishimura T, Tatsumi E, Takaichi S, et al.: Morphologic changes of the aortic wall due to reduced systemic pulse pressure in prolonged non pulsatile left heart bypass. Asaio Journal 1997;43:M691-M5.
30. Birukov KG, Shirinsky VP, Stepanova OV, et al.: Stretch Affects Phenotype and Proliferation of Vascular Smooth-Muscle Cells. Mol Cell Biochem 1995;144:131-9.
31. Slaughter MS, Tsui SS, El-Banayosy A, et al.: Results of a multicenter clinical trial with the Thoratec Implantable Ventricular Assist Device (vol 133, pg 1573, 2007). J Thorac Cardiov Sur 2007;134:34a-a.
32. Vignon-Clementel IE, Figueroa CA, Jansen KE, Taylor CA: Outflow boundary conditions for three-dimensional finite element modeling of blood flow and pressure in arteries. Comput Method Appl M 2006;195:3776-96.
33. Arzani A, Suh GY, Dalman RL, Shadden SC: A longitudinal comparison of hemodynamics and intraluminal thrombus deposition in abdominal aortic aneurysms. Am J Physiol-Heart C 2014;307:H1786-H95.
34. Mano Y, Takehara Y, Sakaguchi T, et al.: Hemodynamic Assessment of Celiaco-mesenteric Anastomosis in Patients with Pancreaticoduodenal Artery Aneurysm Concomitant with Celiac

Artery Occlusion using Flow-sensitive Four-dimensional Magnetic Resonance Imaging. Eur J Vasc Endovasc 2013;46:321-8.

35. Menon AK, Dohmen G, Mahnken AH, Autschbach R: Successful combined procedure of HeartMate II left ventricular assist device implantation and minimally invasive transapical aortic valve replacement. J Thorac Cardiov Sur 2011;142:708-9.

Table 1: Measured echocardiographic velocities at different LVAD inflows and computed flow splits for each branch of the abdominal aorta according to vessel diameter of patient case A.

	LGA	CHA	SA	MA	RRA	LRA	AA
CO= 4 [L/min]							
Velocity [cm/s]	9.8	15.5	31.4	34.3	15.6	17.1	37.2
Flow division [%]	1.5	2.5	11.9	13.1	2.5	2.8	48.2
CO= 5 [L/min]							
Velocity [cm/s]	20.1	22.2	29.0	45.1	22.4	18.2	45.0
Flow division [%]	2.8	3.1	9.4	14.6	3.2	2.4	49.2
CO= 6 [L/min]							
Velocity [cm/s]	33.8	47.0	53.2	70.1	45.9	43.0	43.9
Flow division [%]	3.6	5.2	13.6	19.9	4.9	4.7	37.3

Note: CO = Cardiac Output; LGA = left gastric artery; CHA = common hepatic artery; SA = splenic artery; MA = mesenteric artery; RRA = right renal artery; LRA = left renal artery; AA = abdominal artery

Table 2: Mean (± standard deviation) of flow velocity and shear stress computed in the celiac trunk and other aortic branches

	LGA	CHA	SA	MA	RRA	LRA	AA
Velocity [m/s]	0.57±0.25	0.52±0.17	0.32±0.06	0.81±0.28	0.24±0.08	0.61±0.73	0.26±0.12
WSS [Pa]	9.08±5.45	4.58±1.77	6.34±2.65	8.16±3.88	2.63±0.95	5.73±6.32	2.14±1.89

Note: LGA = left gastric artery; CHA = common hepatic artery; SA = splenic artery; MA = mesenteric artery; RRA = right renal artery; LRA = left renal artery; AA = abdominal artery

Figure 1

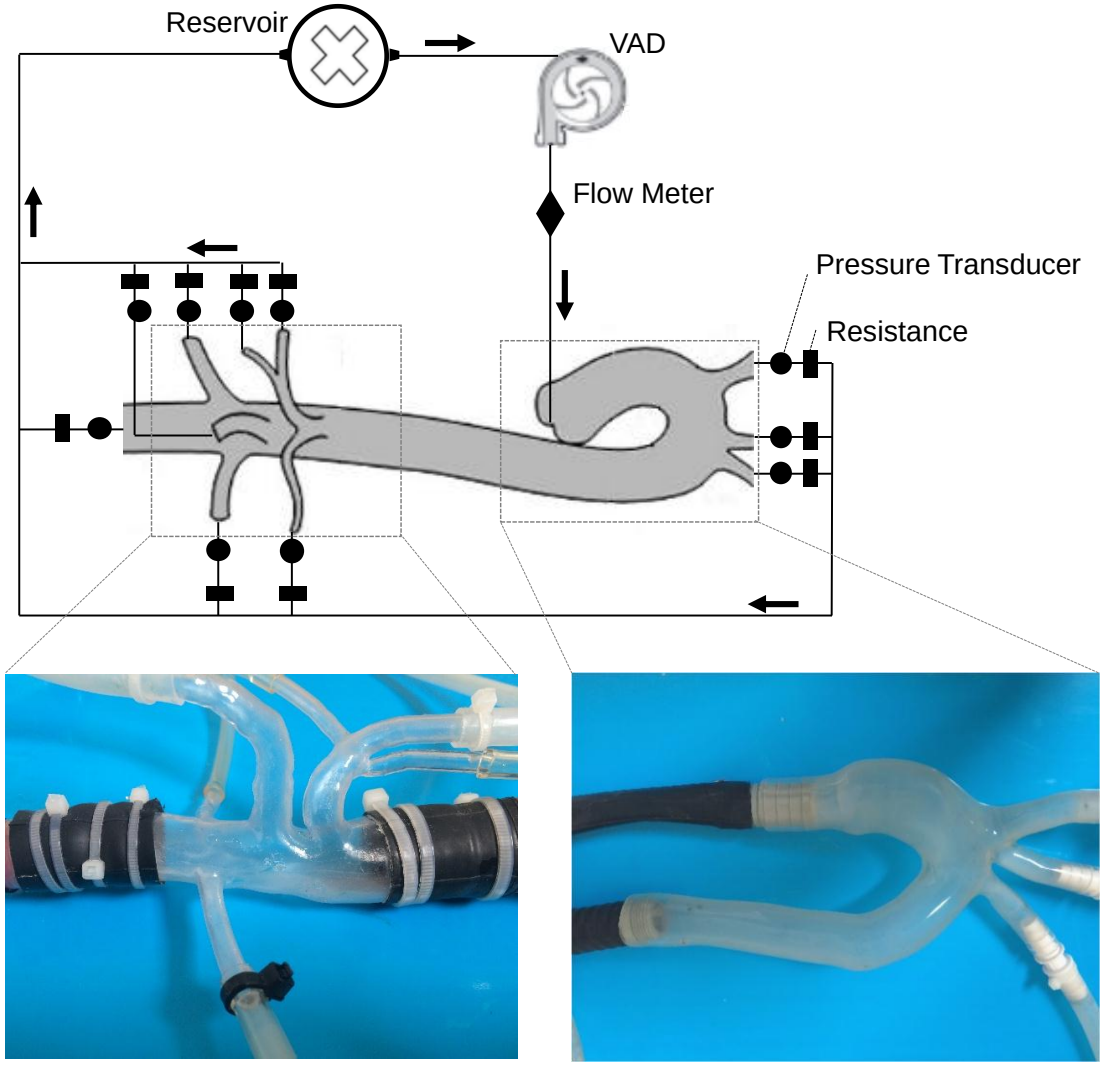

Figure 2

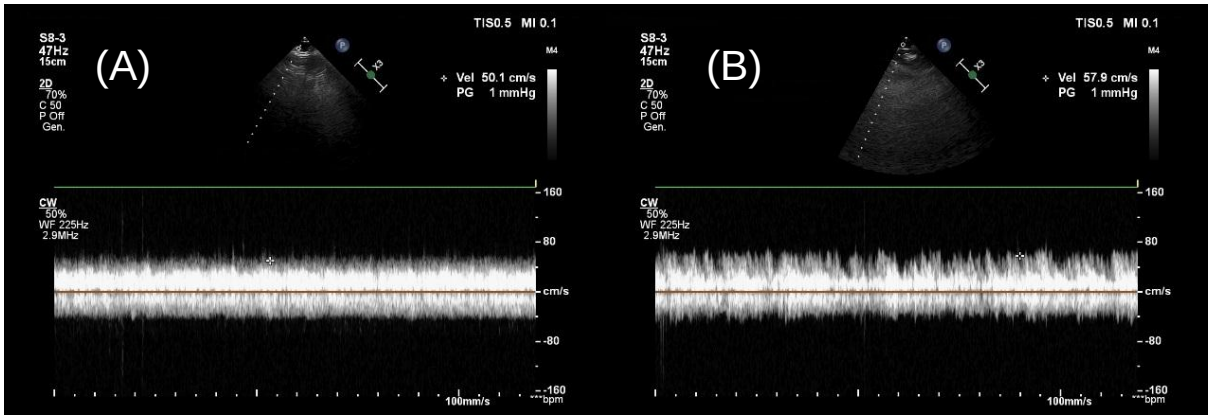
(A)
S8-3
47Hz
15cm
2D
70%
C 50
P Off
Gen.
TIS0.5 MI 0.1
M4
Vel 50.1 cm/s
PG 1 mmHg
CW
50%
WF 225Hz
2.9MHz
160
80
cm/s
-80
-160
100mm/s
bpm
(B)
S8-3
47Hz
15cm
2D
70%
C 50
P Off
Gen.
TIS0.5 MI 0.1
M4
Vel 57.9 cm/s
PG 1 mmHg
CW
50%
WF 225Hz
2.9MHz
160
80
cm/s
-80
-160
100mm/s
bpm

Figure 3

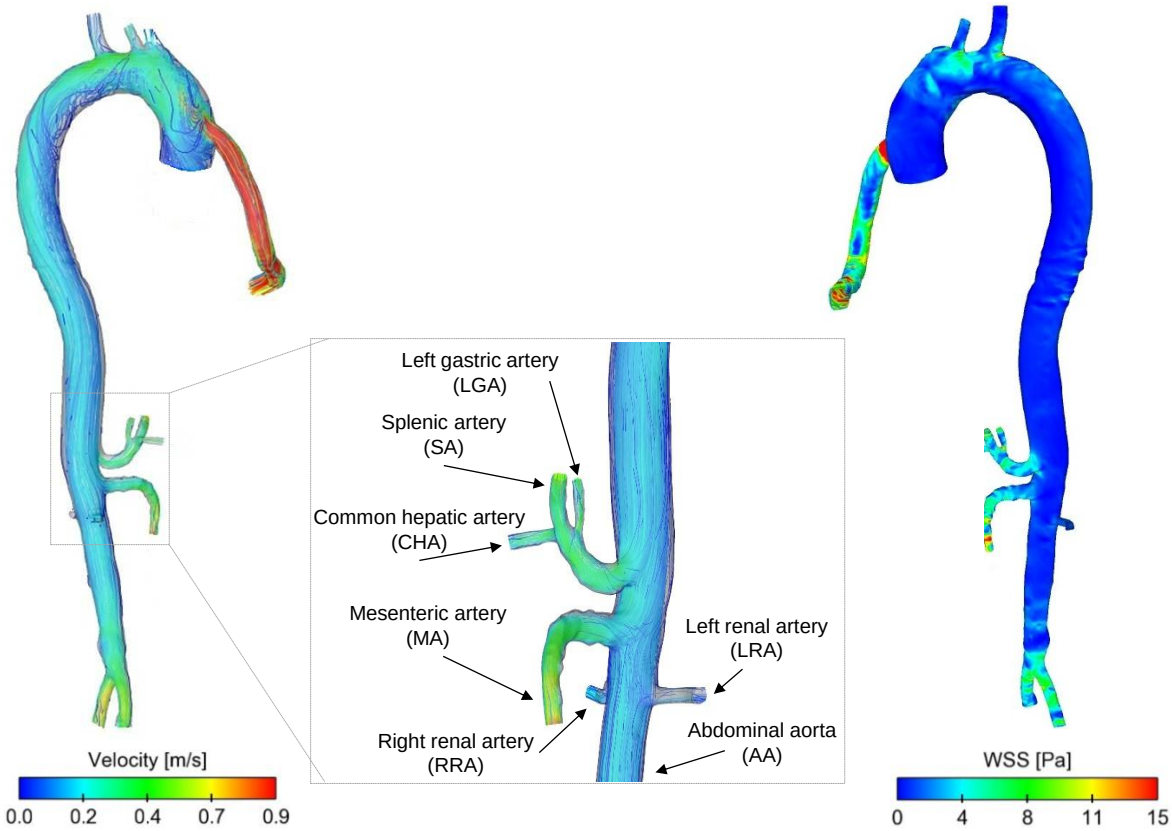
Left gastric artery
(LGA)
Splenic artery
(SA)
Common hepatic artery
(CHA)
Mesenteric artery
(MA)
Left renal artery
(LRA)
Right renal artery
(RRA)
Abdominal aorta
(AA)
Velocity [m/s]
0.0 0.2 0.4 0.7 0.9
WSS [Pa]
0 4 8 11 15

Figure 4

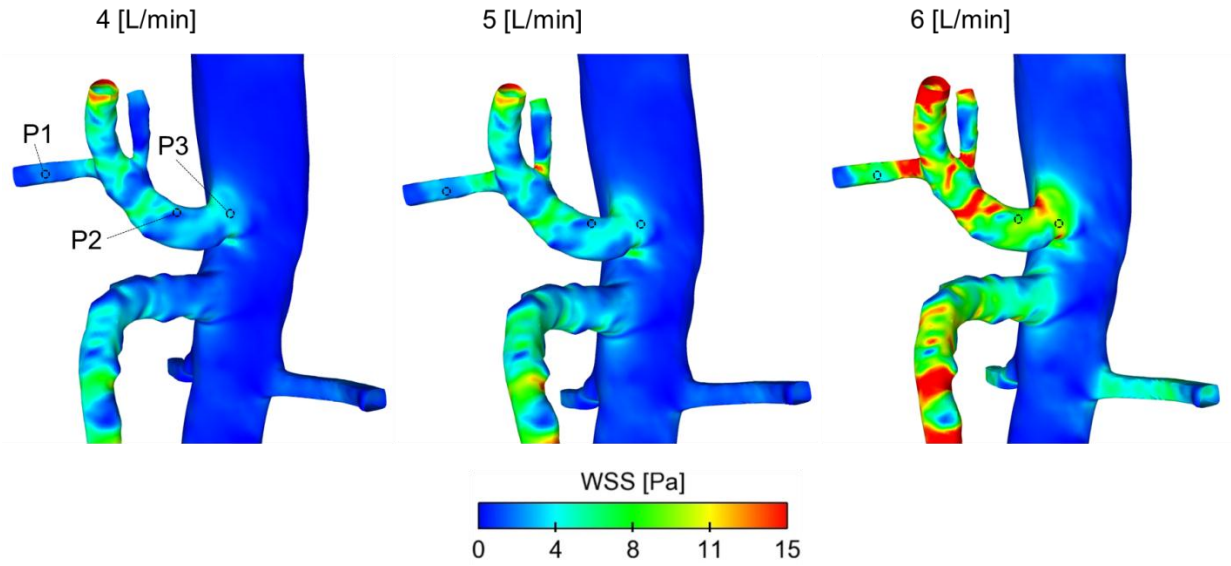

Figure 5

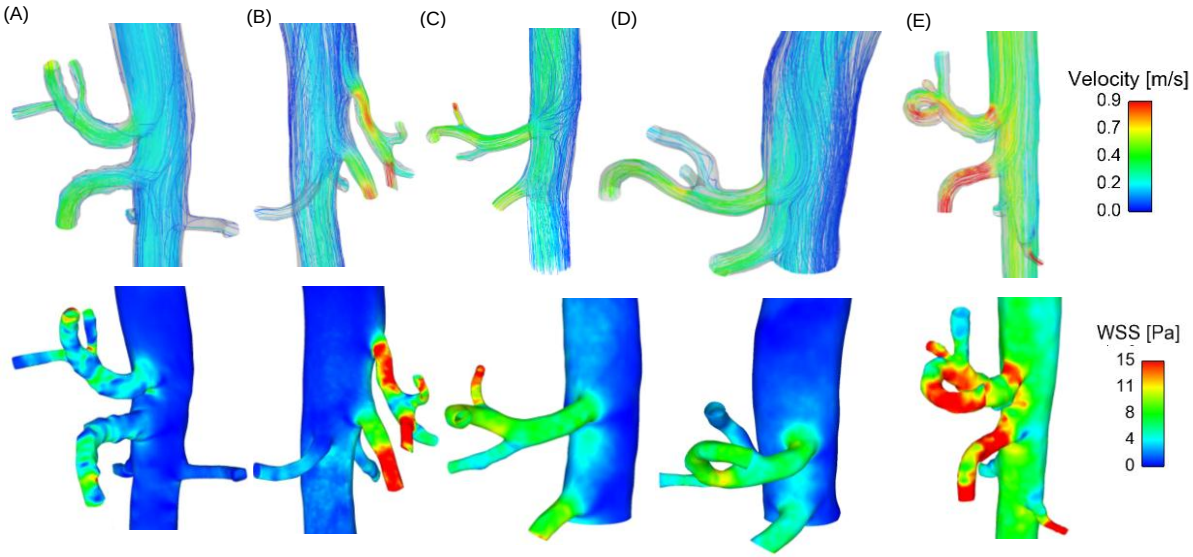

Figure 6

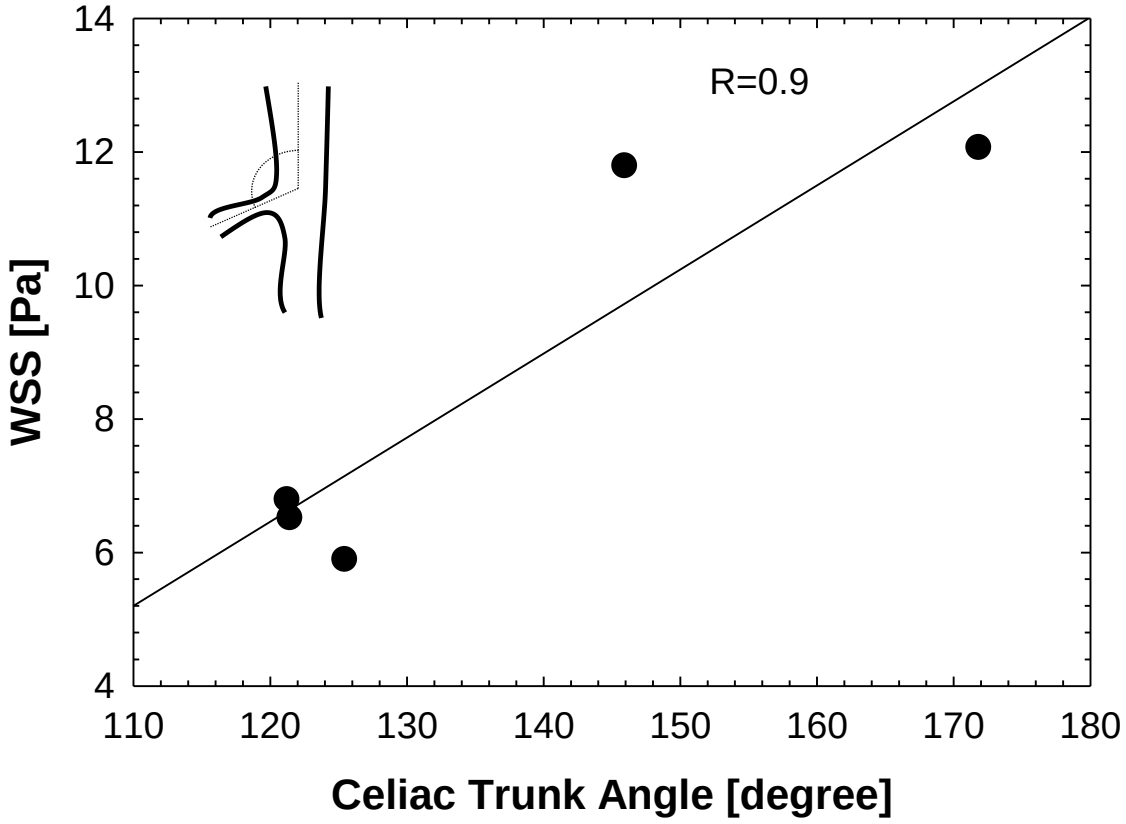
14
12
10
8
6
4
WSS [Pa]
R=0.9
110
120
130
140
150
160
170
180
Celiac Trunk Angle [degree]

MOX Technical Reports, last issues

Dipartimento di Matematica
Politecnico di Milano, Via Bonardi 9 - 20133 Milano (Italy)

47/2016 Canuto, C.; Nochetto, R. H.; Stevenson R.; Verani, M.
On p-Robust Saturation for hp-AFEM

46/2016 Lila, E.; Aston, J.A.D.; Sangalli, L.M.
Smooth Principal Component Analysis over two-dimensional manifolds with an application to Neuroimaging

45/2016 Bukac, M.; Yotov, I.; Zunino, P.
DIMENSIONAL MODEL REDUCTION FOR FLOW THROUGH FRACTURES IN POROELASTIC MEDIA

42/2016 Iannetti, L.; D'Urso, G.; Conoscenti, G.; Cutri, E.; Tuan, R.S.; Raimondi, M.T.; Gottardi, R.; Zu
Distributed and lumped parameter models for the characterization of high throughput bioreactors

43/2016 Ambrosi, D.; Ciarletta, P.; De Falco, C.; Taffetani, M.; Zunino, P.
A multiscale modeling approach to transport of nano-constructs in biological tissues

44/2016 Notaro, D.; Cattaneo, L.; Formaggia, L.; Scotti, A.; Zunino, P.
A Mixed Finite Element Method for Modeling the Fluid Exchange between Microcirculation and Tissue Interstitium

40/2016 Miglio, E.; Parolini, N.; Penati, M.; Porcù R.
High-order variational time integrators for particle dynamics

39/2016 Andrà, C.; Brunetto, D.; Parolini, N.; Verani, M.
Student interactions during class activities: a mathematical model

38/2016 Quarteroni, A.; Manzoni, A.; Vergara, C.
The Cardiovascular System: Mathematical Modeling, Numerical Algorithms, Clinical Applications

41/2016 Giovanardi, B.; Scotti, A.; Formaggia, L.
A hybrid XFEM - Phase Field (Xfield) method for crack propagation in brittle materials